C. R. Physique 16 (2015) 741–757

Contents lists available at ScienceDirect

Comptes Rendus Physique

www.sciencedirect.com

Prix Gustave-Ribaud 2014 de l'Académie des sciences

Instability-driven quantum dots

Instabilité et boîtes quantiques

Jean-Noël Aqua [a,*], Thomas Frisch [b]

[a] *Institut des nanosciences de Paris, UPMC (Université Paris-6), CNRS, UMR 7588, 4, place Jussieu, 75005 Paris, France*
[b] *Institut Non Linéaire de Nice, Université de Nice Sophia Antipolis, UMR, CNRS 6618, 1361, routes des Lucioles, 06560 Valbonne, France*

ARTICLE INFO

Article history:
Available online 4 September 2015

Keywords:
Strained film
Morphological instability
Epitaxy

ABSTRACT

When a film is strained in two dimensions, it can relax by developing a corrugation in the third dimension. We review here the resulting morphological instability that occurs by surface diffusion, called the Asaro–Tiller–Grinfel'd instability (ATG), especially on the paradigmatic silicon/germanium system. The instability is dictated by the balance between the elastic relaxation induced by the morphological evolution, and its surface energy cost. We focus here on its development at the nanoscales in epitaxial systems when a crystal film is coherently deposited on a substrate with a different lattice parameter, thence inducing epitaxial stresses. It eventually leads to the self-organization of quantum dots whose localization is dictated by the instability long-time dynamics. In these systems, new effects, such as film/substrate wetting or crystalline anisotropy, come into play and lead to a variety of behaviors.

RÉSUMÉ

Un film qui subit une pression selon deux dimensions peut relaxer cette contrainte en ondulant dans la troisième dimension. Nous analysons ici l'instabilité morphologique qui en résulte grâce à la diffusion de surface, l'instabilité d'Asaro–Tiller–Grinfel'd (ATG), en particulier sur le système paradigmatique silicium/germanium. L'instabilité est régie par l'équilibre entre la relaxation élastique liée à l'évolution de la surface, et son coût en énergie de surface. Nous nous focalisons ici sur sa manifestation aux échelles nanométriques dans les systèmes épitaxiés, quand un film cristallin est déposé sur un substrat de paramètre de maille différent, induisant une contrainte élastique bi-axiale. Cette évolution débouche aux temps longs sur l'auto-organisation de boites quantiques dont la localisation est dictée par la dynamique aux temps longs. Dans ces systèmes, des nouveaux effets entrent en jeu, comme le mouillage entre le film et son substrat ou l'anisotropie cristalline, et débouchent sur une diversité de comportements nouveaux.

* Corresponding author.
E-mail address: Jean-Noel.Aqua@insp.jussieu.fr (J.-N. Aqua).

http://dx.doi.org/10.1016/j.crhy.2015.08.002
1631-0705/

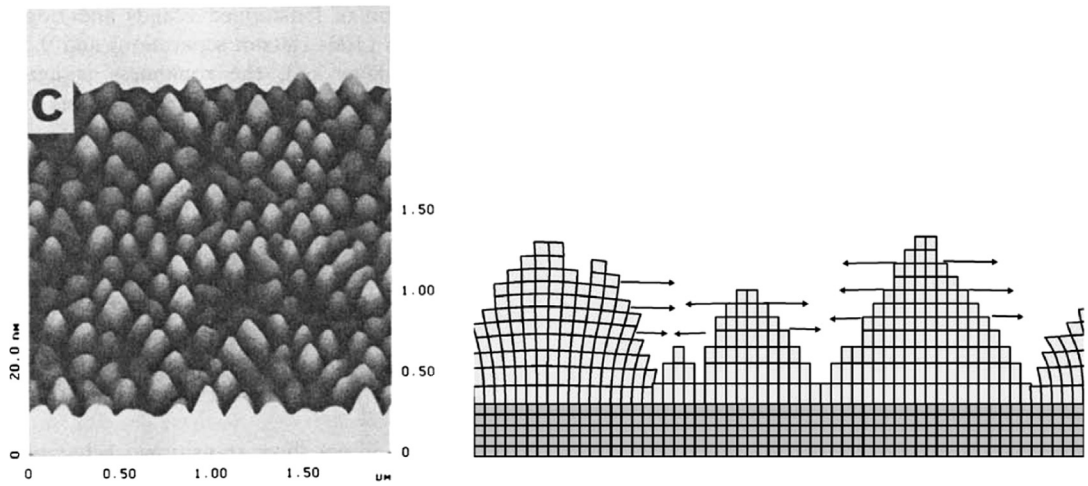

Fig. 1. Seminal observation of the ATG instability on SiGe [14] and schematic representation of the strain relaxation allowed by a morphological evolution, from [18].

1. Introduction

Quantum dots are nowadays common objects, easy to fabricate, manipulate and use on an everyday laboratory life basis. These objects, which keep charge carriers in a structure with dimensions smaller or of the order of the de Broglie wavelength, exhibit quantum confinement effects. After the technological revolution introduced by the transistor in the late 1940s, which resulted in our information-based societies, the development of such quantum confining nanostructures contain the seeds of strong technologic and scientific progress [1–3] (and references therein).

The first quantum nanostructures to be proposed and realized are quantum wells that confine charge carriers in one dimension and led to the 2000 Nobel Prize awarded to Alferov and Kroemer [4,5]. They found many applications in laser diodes for, e.g., compact disc readers or fiber optic transmitters, and more recently in the blue laser diodes that led to the 2014 Nobel Prize awarded to Akasaki, Amano and Nakamura [6]. In a 'quantum wire', such as a carbon nanotube, electrons are confined in two dimensions, but are free to move in one direction; in a 'quantum dot' or 'artificial atom', electrons are confined in all directions, which leads to a discrete energy spectrum. Quantum dots are thence used in labs for producing single photons and entangled photons, quantum computing devices, single-electron transistors, and are even already embedded in television displays first commercialized in 2013.

Quantum dots (QD) may be produced with different techniques, in colloidal solutions or in semiconductor epitaxy. If lithography is used in relatively large structures, the control of crystal growth down to a few nanometers allows the in-situ self-organization of defect-free nanostructures when a thin film is coherently deposited on a substrate. This growth exemplifies the general trend towards self-organization in out-of-equilibrium systems, which is commonly associated with the so-called Stranski–Krastanov growth, specific to epitaxial systems and explained in the following. Its driving force is the relaxation of the stress induced by the lattice mismatch between a film and its substrate, while it is hindered by the surface energy cost and by wetting effects between a film and a substrate. At the temperatures where QD grow, only surface mass transfers are activated and lead to surface corrugation. This evolution should thence not be confused with the buckling of a strained film, which involves the movement of the full system.

In some growth conditions, QD growth occurs without nucleation and results from a morphological instability, the ATG instability, proposed by Asaro and Tiller [7] and then Grinfel'd [8]. It was experimentally demonstrated in ^{4}He films in Balibar's group [9–11], and also in polymer films [12]. In semi-conductors' epitaxy, it was evidenced in indium–gallium–arsenic systems [13] and in silicium–germanium (SiGe) films [14,15]. However, QDs result mostly in the long-time dynamics of the instability, where numerous effects come into play, especially wetting interactions between the film and its substrate, crystalline anisotropy, but also non-linear effects. The goal of the present article is to review the different results that may be drawn theoretically for this instability, and to compare them with experimental knowledge.

2. Asaro–Tiller–Grinfel'd instability

The Asaro–Tiller–Grinfel'd instability occurs when a strained film relaxes by developing a surface corrugation, see, e.g., [16,17] for a review and Fig. 1. In hetero-epitaxial systems, strain occurs when a film is coherently deposited on a substrate with a different lattice parameter. Hence, the film experiences a bi-dimensional strain in the substrate plane that already leads to a Poisson dilatation in the growth direction. The morphological evolution then happens via surface diffusion driven by elastic relaxation. The description of the ATG instability is merely ruled by surface diffusion enforced by the surface chemical potential density μ that includes capillary and elastic effects. We consider a regular film surface lo-

cated at $z = h(\boldsymbol{r}, t)$, where $\boldsymbol{r} = (x, y)$. When atoms are deposited on the surface with a given flux F and then diffuse, mass conservation enforces the diffusion equation [19]:

$$\frac{\partial h}{\partial t} = D\sqrt{1+|\nabla h|^2}\,\boldsymbol{\Delta}_{\mathrm{S}}\mu + F\,. \tag{1}$$

Here, $\boldsymbol{\Delta}_{\mathrm{S}}$ is the surface Laplacian [20] which is merely the bi-dimensional Laplacian $\boldsymbol{\Delta} = \partial^2/\partial x^2 + \partial^2/\partial y^2$ in the small-slope approximation used in the following, which is relevant to the experiments described below. The diffusion coefficient D in (1) involves the atomic diffusion coefficient D_{a}, but also the atomic volume Ω and the surface density of lattice sites ν [21], $D = D_{\mathrm{a}}\dfrac{\nu\,\Omega^2}{k_{\mathrm{B}}\,T}$, neglecting local lattice expansion effects and vacancy concentration [19]. In fact, D is supposed to be a constant in the derivation of (1) [19], independent, e.g., of the local surface orientation, or of the local strain. This strong hypothesis is also related to the continuum framework underlying Eq. (1) that is used here. It is justified in SiGe systems as the (001) substrate orientation on which the instability is observed always displays some roughness, see Fig. 3. It may be rationalized by the fact that this orientation is a stable but not a facet orientation, consistently with the nucleationless evolution of the ATG instability [22] explained in the following.

The chemical potential density used in (1) may be computed by a virtual addition of mass on the surface in terms of functional derivative $\mu(\boldsymbol{r}) = \dfrac{\delta\mathcal{F}}{\delta h}(\boldsymbol{r})$, where the free energy $\mathcal{F}$ depends on the shape $h(\boldsymbol{r})$. It contains two contributions, $\mathcal{F} = \mathcal{F}^{\mathrm{el}} + \mathcal{F}^{\mathrm{s}}$. The surface energy $\mathcal{F}^{\mathrm{s}} = \int \gamma\,\mathrm{d}^2S$ with the surface area element d^2S, includes different effects. Its basic definition describes the energetic cost of creation of a surface when γ is constant. But γ is function of the local orientation of the crystal, describing the fact that different orientations do not have the same cost. This well-known property is usually associated at equilibrium with the Wulff construction [23]. In addition, the surface energy, which is an excess quantity, is also a function of the local environment of atoms. In the case of interest here, where an atomically thin film is deposited onto a substrate, the later environment naturally depends on the film thickness, $\gamma = \gamma(h)$ [24,25]. This effect is at the origin of a critical thickness for the development of the instability and of the stabilization of a wetting layer between islands, as seen in the following. A priori, we stick in this section to the basic case where γ is merely a constant, so that one finds

$$\mu^{\mathrm{s}}(\boldsymbol{r}) = \gamma\,\kappa(\boldsymbol{r})\,, \tag{2}$$

where $\kappa(\boldsymbol{r})$ is the mean curvature [26], which is $-\partial^2 h/\partial x^2 - \partial^2 h/\partial y^2 + \mathcal{O}(\nabla h^3)$ when the surface slopes are small.

The elastic contribution $\mathcal{F}^{\mathrm{el}}$ is a priori a non-local functional of the surface shape $h(\boldsymbol{r})$, describing the long range of elastic interactions. The latter results from the lattice mismatch between the film and the substrate when the epitaxy is coherent, which is the case for thin SiGe systems, at least in the first stages of the morphological evolution (dislocation may occur in large domes or superdomes that arise for thick enough films). The dynamics occurs on time scales that are large compared to the time scales for relaxation towards mechanical equilibrium. Hence, one should look for the displacements that solve the mechanical equilibrium equations. As a first and relevant approximation, one could consider in SiGe systems elasticity as linear and isotropic. Moreover, when the system is coherent, one should also impose the continuity of displacements and forces at the film/surface boundary, while the film's upper surface should be considered as free of stress (neglecting also surface stress effects [27]). If one can find exact solutions for the elastic field in two dimensions using complex decompositions, see, e.g., [28], the solution for the elastic field is not known in the general case in three dimensions. However, one may find an exact solution when the surface slopes are small. This hypothesis is not very restrictive: it is certainly relevant to describe the instability initial stage where the surface departs only slightly from its initial flat configuration, but it is also at work in the mature stage of the instability where quantum dots arise that initially develop only slopes of at most 11° for (105) facets. In the small slope approximation, one may find the solution for the elastic displacements, and thence for the elastic chemical potential density at first order

$$\mu^{\mathrm{el}} = \mathcal{E}_0\left\{1 - 2(1+\nu)\left[\mathcal{H}_{xx}(h) + \mathcal{H}_{yy}(h)\right]\right\}\,, \tag{3}$$

where ν is the Poisson's ratio and $\mathcal{E}_0 = Ym^2/(1-\nu)$, the elastic energy density of a flat film with a Young modulus Y and a misfit m with its substrate. The Hilbert operators involved in (3) are given in the Fourier space along (x, y) by $\mathcal{H}_{ij}(h) = \mathrm{TF}^{-1}\left[(k_i k_j/|\boldsymbol{k}|)\,\mathrm{TF}[h]\right]$, with the 2D wave-vector $\boldsymbol{k}$, so that $\mathcal{H}_{xx} + \mathcal{H}_{yy}$ acts merely as $\mathcal{H}_{xx}(h) + \mathcal{H}_{yy}(h) = \mathrm{TF}^{-1}\left[|\boldsymbol{k}|\,\mathrm{TF}(h)\right]$.

ATG instability results from the competition between the elastic relaxation described by (3) and the capillary energy cost described by (2). It is already characterized by the length scale

$$l_0 = \frac{\gamma}{2(1+\nu)\mathcal{E}_0}\,, \tag{4}$$

which is typically 13 nm for a $Si_{0.7}Ge_{0.3}$ film on Si [29]. It is associated with the time scale $t_0 = l_0^4/D\gamma$, which is typically 270 s in the same conditions. From now on, lengths and time are given in units of these scales. One may solve the evolution equation (1) by considering a linear analysis where the film-free surface is decomposed into Fourier modes along x and y. One finds an exponential growth $h(\boldsymbol{r}) = \bar{h} + h_1 \mathrm{e}^{-\mathrm{i}\boldsymbol{k}\cdot\boldsymbol{r}}\mathrm{e}^{\sigma(\boldsymbol{k})t}$ with

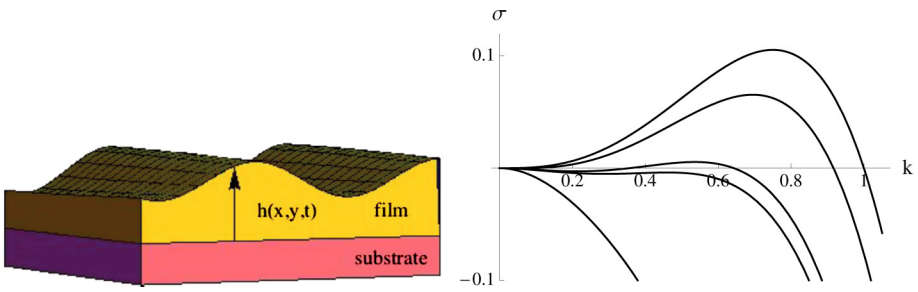

Fig. 2. (Color online.) (Left) Film/substrate geometry characterized by a flat interface and a corrugated free surface defined by $z = h(\mathbf{r})$. (Right) Growth rate σ of an harmonic corrugation with a wavevector $\boldsymbol{k}$ as a function of $\boldsymbol{k}$ for different film thicknesses: the top curve corresponds to the generic ATG growth rate given in Eq. (5), corresponding to the thick film limit when wetting is at play; when the film mean thickness decreases while wetting is at play, the growth rate σ decreases and remains negative for a thickness lower than the critical thickness h_c.

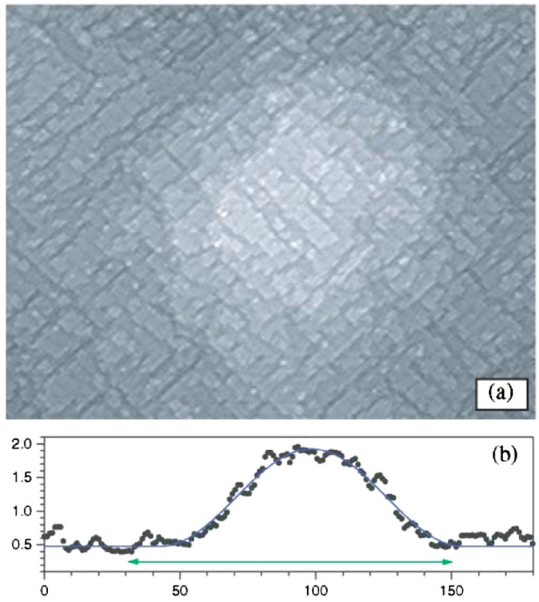

Fig. 3. (Color online.) STM image and line scan of the surface of a $Si_{0.5}Ge_{0.5}$ film on Si(001) displaying both the wetting layer and a small mound [22].

$$\sigma(\boldsymbol{k}) = |\boldsymbol{k}|^3 - \boldsymbol{k}^4, \tag{5}$$

in dimensionless units (i.e. $1/l_0$ for k), see Fig. 2. This growth rate is positive for the full range of modulus $|\boldsymbol{k}| \leq 1$. Hence, an initial film corrugation with a white noise will amplify all the long-wave contributions, and especially the maximum at $|\boldsymbol{k}|_{\max} = 3/4$. The resulting morphological configuration is typically displayed in Fig. 4, which corresponds to the solution for h given by (5) and an initial white noise. Similarly to experiments [17], one finds that the relaxation associated with the instability can be quite small, see Fig. 4, even though it drives the film's evolution. Note that it can even be tailored, e.g., using tensilely strained pseudo-substrates, in order to prevent the instability development and grow coherent, thick and flat layers without a noticeable morphological evolution [30,31].

It should be noticed that in semi-conductors epitaxy, surface diffusion and strain relaxation may lead to two different phenomena that should not be confused, see Fig. 5: either the nucleationless evolution [32] described by the morphological ATG instability, or an evolution dictated by nucleation and characterized by an abrupt 2D/3D transition, see, e.g., [33,25,34]. The competition between the two pathways is dictated by the amplitude of the lattice misfit: nucleation occurs when the misfit is large enough to lead to a strong elastic energy relaxation, typically on Ge films on Si, while the instability occurs at low misfit, e.g., on a $Si_{1-x}Ge_x$ film on Si(100) where $x \lesssim 0.5$. In the latter case, the elastic relaxation is too small so that the nucleation barrier for the nucleation of an island is too large. This competition was demonstrated in kinetic Monte Carlo simulations including elastic and capillary effects [35], and is also possible because the SiGe(100) surface is rough enough [22,36].

The instability linear regime mentioned above is relevant to describe the first stage of the morphological evolution of a strained film. However, the exponential solution to this linear regime cannot grow forever as slopes get larger and non-linear effects come into play. The fate of the instability is then singular in the basic description of the instability, i.e. with the ingredients mentioned so far to get (5) (i.e. in particular, with a constant γ, no wetting interactions, etc.). Both in 2D and

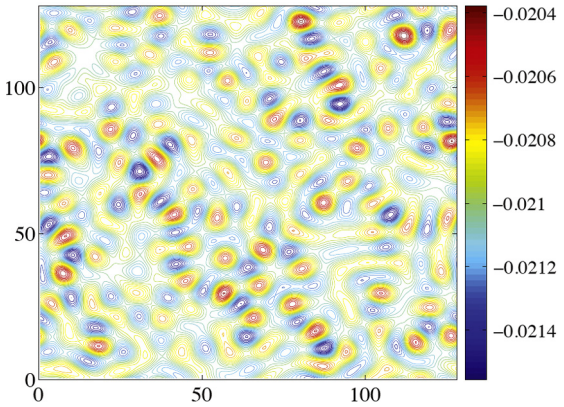

Fig. 4. (Color online.) Solution to the Asaro–Tiller–Grinfel'd instability problem given by the growth rate (5) and an initial white noise. The color field describes the strain level around −0.021, the strain corresponding to a $Si_{0.7}Ge_{0.3}$ film on Si, which displays only small variations.

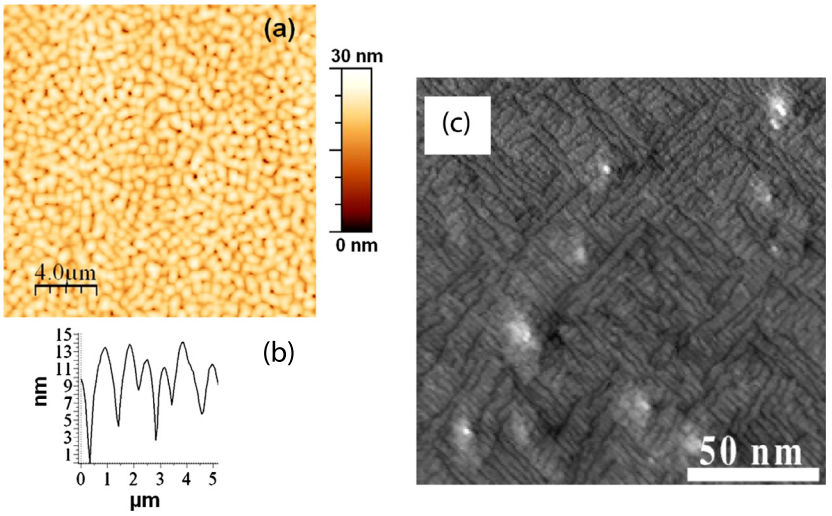

Fig. 5. (Color online.) (a) and (b) ATG instability on a $Si_{0.85}Ge_{0.15}$ film on Si(100): (a) top view and (b) side view, from [37]; (c) nucleation of islands on a Ge film on Si(100), from [38].

3D systems, the film dynamics leads to cusps on the surface, which concentrate the elastic stress and allow the rest of the surface to relax its stress [28]. The surface evolution may be numerically integrated using either an analytic solution to elasticity in 2D [39], a 2D Green function valid in the small-slope approximation [40], or a weakly non-linear analysis in 3D [41]. The different analyses lead to the formation of crack-like grooves that quickly transform into cusps and blow-up singularities on the surface for a finite time, see Fig. 6. These singularities are related to the occurrence in experiments of grooves, then cusps and dislocations, see Fig. 7, as evidenced in thick SiGe films [15] or in ^{4}He films [10].

3. ATG instability and wetting

While the ATG instability is associated with a singular dynamics in thick films, it behaves differently in thin films. Indeed, in SiGe films thinner than at most a few tens of nanometers, the ATG instability leads conversely to a regular and smooth evolution that eventually leads to self-organized quantum dots separated by a wetting layer typically 3 monolayers (ML) thick. This striking difference is due mainly to the wetting interactions between the film and its substrate, which are naturally important at low thicknesses. Similar to the wetting interactions between a fluid and a solid, wetting between solids is related to microscopic interactions at the surface. The surface energy, which is an excess energy [42], is indeed function of the local environment around the surface atoms. When one considers the surface energy of a crystal film, one must consider that the environment of surface atoms is crucially dependent on the presence of a substrate a few monolayer beneath or not. Hence, one expects the surface energy to depend on the film's thickness

$$\gamma = \gamma(h/\delta)\,, \tag{6}$$

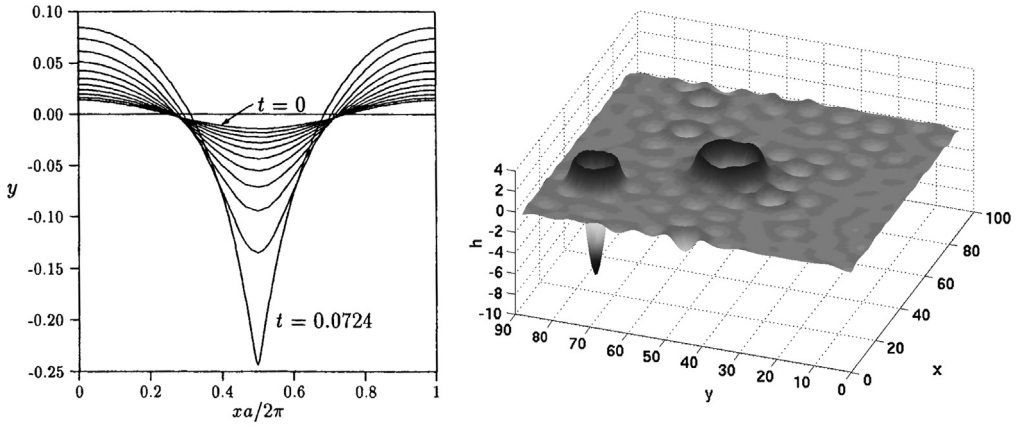

Fig. 6. Long-time dynamics of the ATG instability showing cusps for a finite-time, (left) in 2D [39] and (right) in 3D [41].

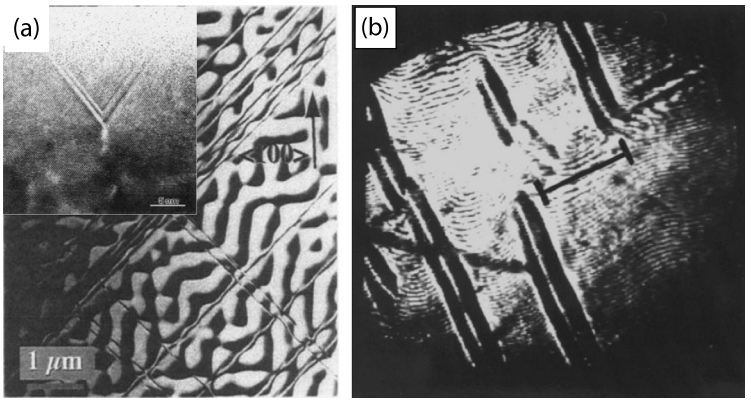

Fig. 7. (a) Dislocation development on top of the ATG instability in thick SiGe films [15], which correspond to cusp production (side view in inset); (b) formation of deep grooves in ^{4}He films [10].

where δ is a few atomic distances and characterizes the interactions between atoms [25,24]. This property may be evidenced by microscopic calculation of surface energies, either based on so-called ab-initio calculations or by pseudo-potential models [43–45]. The results may be well fitted by an exponential decay $\gamma = \gamma_{\mathrm{f}}[1 + c_{\mathrm{w}} \exp(-h/\delta)]$, where γ_{f} is the film usual surface energy while c_{w} and δ characterize the wetting effect. Note that a singular $1/h^n$ dependence may be used, e.g., to model van der Waals bonding at not too small distances, but smooth variations are suited for semi-conductors and metals. Note that wetting introduces symmetry breaking in the problem in the direction of the growth, which is not present a priori in the ATG framework (except from a negligible h dependance that could arise when the film's and the substrate's Poisson ratio and Young modulus differ [26]). Eventually, when such an effect is at work, the functional derivation of the surface chemical potential includes an extra term and reads

$$\mu(\boldsymbol{r}) = \gamma(h)\,\kappa(\boldsymbol{r}) + \frac{\mathrm{d}\gamma}{\mathrm{d}h} n_z + \mu^{\mathrm{el}}(\boldsymbol{r}) + \mu_0\,, \tag{7}$$

where n_z is the projection of the surface unit vector on the growth direction, while μ_0 is the reference chemical potential. The consequences of such an extra dependance are non-perturbative.

The presence of wetting interactions has a first crucial effect as regards the inhibition of the ATG instability below a given critical thickness h_{c}, that is the usual Stranski–Krastanov critical thickness. The latter thickness is characteristic of the Stranski–Krastanov growth mode, which is particular to crystal films compared to liquid films, see Fig. 8. In this mode, growth occurs first as a 2D layer-by-layer growth as wetting interactions enforce a flat film; once the film is thick enough, these interactions vanish and elastic relaxation may occur when the surface morphologically evolves. This phenomenology is captured by the basic description of the ATG instability augmented by wetting interactions. Indeed, the growth rate (5) is not stable with respect to the addition of a perturbation that should add an extra and leading $\boldsymbol{k}^2$ term in σ, due to the presence of the Laplacian in (1). When wetting interactions are considered, the linear evolution of a harmonic corrugation around $\bar{h}$ with a wave-vector $\boldsymbol{k}$ is characterized by a growth rate

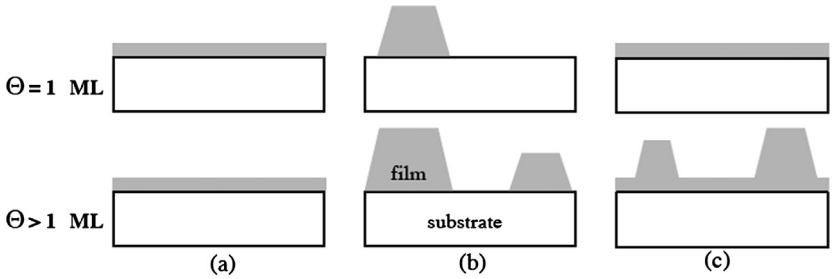

Fig. 8. Different growth modes: (a) 2D layer by layer Franck-van der Merve mode, (b) dewetting and island growth (Volmer–Weber), (c) layer by layer then island growth (Stranski–Krastanov) [18]. The first two modes are similar to the phenomenology of liquid wetting films while the latter mode is particular to crystal growth.

$$\sigma = -\frac{\mathrm{d}^2\gamma}{\mathrm{d}h^2}(\bar{h})\,\boldsymbol{k}^2 + |\boldsymbol{k}|^3 - \boldsymbol{k}^4\,. \tag{8}$$

The $\boldsymbol{k}^2$ term, related to wetting, is negative here when $\mathrm{d}^2\gamma/\mathrm{d}h^2 > 0$, which is the case for an exponentially or algebraically decaying wetting effect. Hence, this negative $\boldsymbol{k}^2$ term reflects the tendency for the film to wet the substrate and thence not to transfer matter on an island by pealing a 2D film. As shown in Fig. 2, which is plotted for an exponential wetting effect, the growth rate σ indeed shifts from a dependance where it is positive for the range of wave-vector where $|\boldsymbol{k}| \leq 1$, mainly for large $\bar{h}$, to a dependance where it is negative for every $\boldsymbol{k}$, i.e. for small $\bar{h}$. In the latter case, the instability is inhibited as all perturbations shrink, so that the surface is not linearly inclined to undergo a morphological evolution. For exponential wetting, one finds a critical height $h_c = -\delta \ln(\delta^2/4c_w)$ below which the instability does not occur and above which it does develop. This consequence is fully consistent with experimental observations. Similarly to the nucleation case, the ATG instability does indeed not occur below a given thickness. This critical thickness usually depends on strain, which may be adjusted by the composition x of the $Si_{1-x}Ge_x$ film. Note that this thickness is usually much smaller than the Matthew's length [46], which corresponds to the critical thickness above which dislocations nucleate in a strained film (i.e. when the elastic energy is too large and overcomes the energy cost for the nucleation of dislocations). In the $Si_{1-x}Ge_x$ system, the Matthew's length is large enough (typically 100 nm for $x \simeq 0.3$) [47] and the morphological evolution is the only strain relieving mechanism for thicknesses between the Stranski–Krastanov critical thickness h_c (typically 3 monolayers) and the Matthew's length.

The second crucial consequence of wetting is the regularization of the instability at long time. Above the critical thickness h_c, the wetting interactions are no longer sufficient to enforce a 2D growth and the ATG instability develops. But as opposed to the thick film's case, its development at long time is no longer characterized by finite-time singularities, cracks or dislocations. On the contrary, after the initial exponential increase, the instability smoothly transforms into islands separated by a wetting layer that continuously evolves. This striking difference was evidenced experimentally during the first observations of the ATG instability [14,48–51]. It occurs while the film is up to a few tens of monolayer thick and the wetting layer spreading between islands is 3 to 4 monolayer thick. For such thin layers, the wetting interactions should be important and naturally associated with the formation of a wetting layer.

On the modeling front, one should investigate the effect of the wetting interactions on the long-time dynamics of the instability, i.e. on the non-linear regime of the instability [52,27,53,54]. Non-linear effects arise in two effects: first, in the wetting potential in (7) if one considers, e.g., an exponentially decreasing wetting potential; second, in the elastic chemical potential, which can be solved exactly at the first non-linear order in the small-slope approximation [53]. The latter non-linear terms arise from the non-linearities associated with the free boundary condition within the linear elasticity framework, and should not be confused with non-linearities that could occur in elasticity at large strain. The non-linear evolution equation during annealing (i.e. without a deposition flux F) eventually reads

$$\begin{aligned}\frac{\partial h}{\partial t} = \Delta\Big\{ &-\left(1 + c_w \mathrm{e}^{-h/\delta}\right)\Delta h - \frac{c_w}{\delta}\mathrm{e}^{-h/\delta}\left(1 - \frac{1}{2}|\nabla h|^2\right) \\ &- \mathcal{H}_{ii}(h) + 2h\Delta h + |\nabla h|^2 + 2\mathcal{H}_{ij}\left[h\,\theta_{ijkl}\mathcal{H}_{kl}(h)\right] + \mathcal{H}_{ij}(h)\theta_{ijkl}\mathcal{H}_{kl}(h)\Big\},\end{aligned} \tag{9}$$

where θ_{ijkl} is a geometric tensor depending on the film's Poisson ratio [53]. The elastic non-linear terms involve the non-local Hilbert operators (3). The elastic contribution, second line in (9), is globally invariant by a shift in the reference height, even though it involves $h\Delta h$ terms, and symmetry breaking in the growth direction is entirely due to wetting. One may investigate numerically the solution to the evolution equation, considering some noise to initiate the instability, either in the initial conditions or during dynamical evolution. One finds that the evolution is regularized by the combination of the non-linear elastic and wetting effects [53]. The cusp-like solutions (Fig. 6), which tend to dig into the film, are avoided by the wetting interactions that prevent the film to be too thin. On the contrary, one finds a smooth and continuous evolution. The initial linear instability, characterized by growing mounds that go deeper into the film, slows down when the film

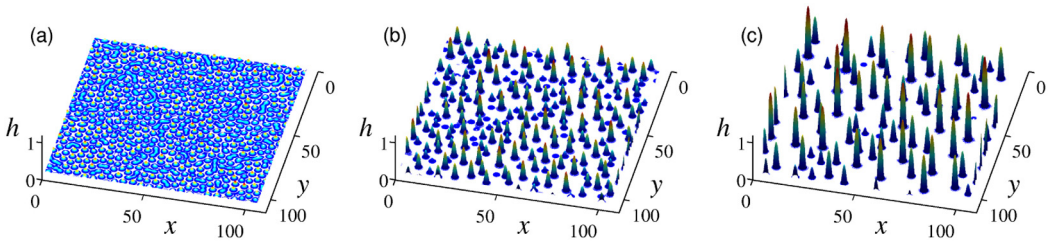

Fig. 9. Non-linear evolution of the ATG instability in presence of wetting, following Eq. (9). Contrary to the thick film case without wetting, the instability leads to the formation of self-organized quantum dots separated by a wetting layer. The snapshots correspond to $t/t_0 = 4$ (left), $t/t_0 = 8$ (center) and $t/t_0 = 14$ (right), from [53].

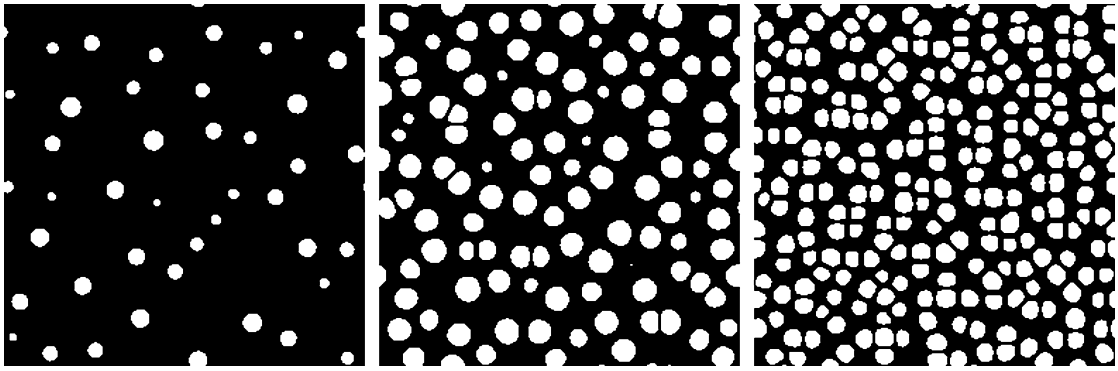

Fig. 10. Different non-linear regimes of the evolution (Eq. (9)) as a function of the deposition flux for (a) low flux $Ft_0 = 4{\cdot}10^{-4}$, (b) intermediate flux $Ft_0 = 0.04$ and (c) large flux $Ft_0 = 0.4$, from [53].

is only a few atomic lengths thick. Then, non-linear wetting effects enforce the spreading of a wetting film between the mounds that evolve into well-defined self-organized islands separated by a wetting layer similarly to experiments, see Fig. 9. As described below, these islands undergo a non-interrupted Ostwald coarsening [53], where the smaller ones disappear to the benefit of the larger ones.

A noticeable feature associated with the symmetry breaking of the dynamical equation (9), is the explicit dependance of the growth on the deposition flux. Indeed, if a deposition term F is added in the r.h.s. of Eq. (9), one finds different growth regimes characterized by a different self-organization, see Fig. 10. When $Ft_0 \ll 1$, the islands resulting at large time are scattered across the surface similarly to the islands that occur during annealing when $F = 0$. However, as F increases, the islands exhibit progressively spatial correlations and gather into clusters, which are well defined when $Ft_0 \gtrsim 0.1$, see Fig. 10. This behavior, which is similar to the trend observed in nucleating islands when F/D increases, does not share the same origin. In the diffusion/nucleation regime, as the diffusion flux increases, the adatoms diffusion length between deposition and nucleation decreases, so that the island density increases with F [55]. In the instability regime however, where the island density results from the balance between the elastic and capillary energies, the increase in the deposition flux acts on coarsening: When growth proceeds quickly, surface diffusion is not active enough to allow the mass transfer between islands that nearly all survive, with an order reminiscent of the initial stages.

4. Crystalline anisotropy

The previous descriptions do not include a crucial factor in crystal growth: crystalline anisotropy. This anisotropy is already responsible for the equilibrium shapes of crystals thanks to the Wulff construction [23], which relates the shape of a crystal to the dependance of its surface energy on the local orientation. This anisotropy may be included in the continuum framework appropriate to describe the instability, by including a surface dependance $\gamma = \gamma(\boldsymbol{n})$, where $\boldsymbol{n}$ is the local normal to the surface [56,16]. In the presence of such a dependance, the functional derivative leads to extra terms in the surface chemical potential that reads,

$$\mu^s(\boldsymbol{r}) = \gamma\,\kappa(\boldsymbol{r}) - \frac{2}{\sqrt{1+|\nabla h|^2}} h_j h_{ij} \frac{\partial \gamma}{\partial h_i} - \sqrt{1+|\nabla h|^2}\, h_{ij} \frac{\partial^2 \gamma}{\partial h_i \partial h_j}\,. \tag{10}$$

A first consequence of this anisotropy on the ATG instability is the dependance of the growth rate σ on the substrate's stiffness. Indeed, the $-\boldsymbol{k}^4$ capillary term in (5) becomes $-\tilde{\gamma}\,\boldsymbol{k}^4$ in the presence of anisotropy, with stiffness $\tilde{\gamma} = \left[\gamma + \partial^2\gamma/\partial h_x^2 + \partial^2\gamma/\partial h_y^2\right]/\gamma$. Hence, a large stiffness value will diminish the growth rate σ and may kinetically prevent the instability from occurring. Because of the initial exponential increase in the instability, the dependance of the

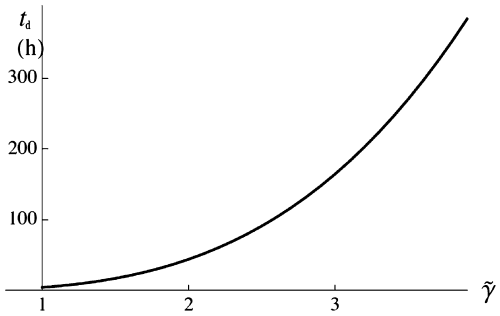

Fig. 11. Typical time t_d for the onset of the instability (defined by a given threshold for the surface roughness) as a function of the surface stiffness $\tilde{\gamma}$, from [37].

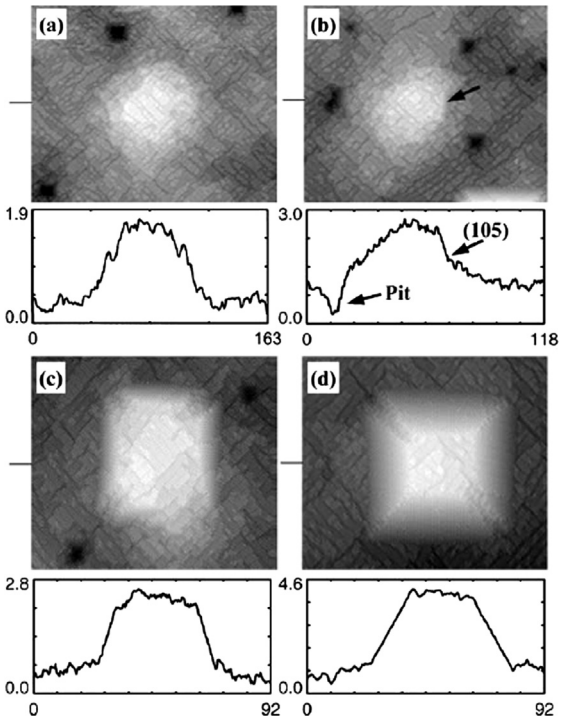

Fig. 12. Evolution from rough mounds to a pyramids on a SiGe film on Si(100), from [60].

instability onset on the surface stiffness is quite important, see Fig. 11. This result may be used to support the experimental difference between the growth on Si(100) and on Si(111). Indeed, one finds that the ATG instability develops on Si(100), while it is inhibited on Si(111), during growth and even during long-time annealing [50,37]. One knows that the (111) orientation on SiGe systems is much stiffer than (100) orientation, which displays an intrinsic roughness [57,58,22,59]. The inhibition on Si(111) may thence be attributed to such a retardation due to the surface stiffness, contrary to the easy evolution on (100).

A second consequence of this anisotropy concerns the island shapes in the ripening regime. If the first islands to grow on Si(100) are rough and rather isotropic mounds, called pre-pyramids, they evolve after some time into square-base and rectangular-base pyramids with (105) facets [48,50,32,60], see Fig. 12. The resulting (105) pyramids are similar to the ones observed in the seminal work on the nucleation regime on pure Ge on Si [61], see Fig. 13. This pre-pyramid-to-pyramid transition corresponds to a first-order transition that occurs when the island volume is large enough (which occurs as coarsening leads to the growth of some islands) [22]. Depending on the growth parameters, the pyramids may then evolve into domes and super-domes when the film is thick enough and/or during a long-enough annealing time [17], similar again to the islands grown in the nucleation regime [62], see Fig. 14.

In order to describe the formation of faceted objects in the ATG instability, one can include an ad-hoc dependance of γ on $\boldsymbol{n}$ with specific orientations [64–69]. The latter should account for the intrinsic roughness of the (100) orientation [22], together with the presence of the well-defined (105) facets. Thanks to the Wulff construction, one knows that facets are associated with cusps in the γ-plot of the materials, i.e. in the function $\gamma(\boldsymbol{n})$. Such singularities cannot be described within a

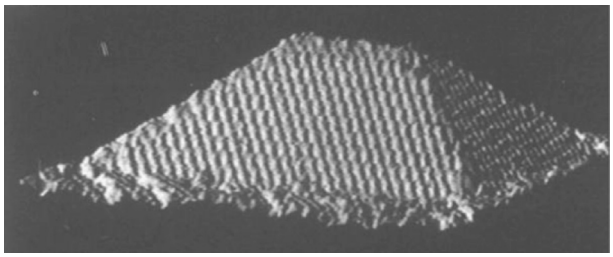

Fig. 13. Pyramid island with (105) facets nucleated on a Ge on Si film, from [61].

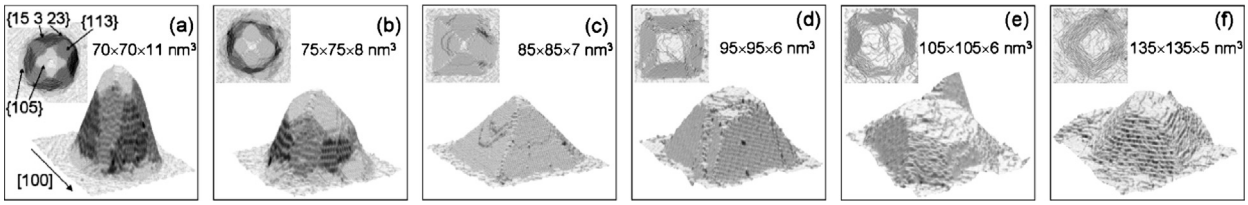

Fig. 14. Different shapes of self-organized quantum dots on SiGe, from [63].

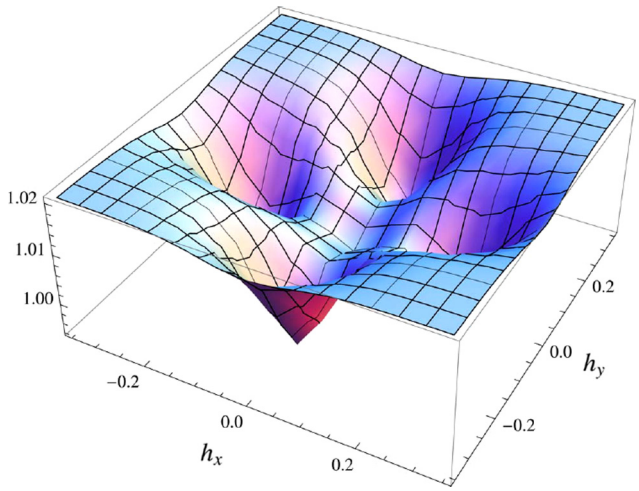

Fig. 15. (Color online.) Typical gamma-plot for SiGe systems displaying the dependance of the surface energy γ on the local orientation given by the slopes h_x and h_y, from [70].

differential framework, but singular orientations can nevertheless be described with ad-hoc regularizations amenable within a differential framework, see, e.g., [64–69]. In order to describe SiGe systems, one may consider a regularized gamma-plot with a shallow minimum near (100) and stiff minima for the (105) orientations [70], see Fig. 15.

The evolution of the ATG instability accounting for such a surface energy anisotropy [71] captures the experimental evolution. The first islands to grow are mainly isotropic mounds. Some of them grow and increase their aspect ratio and side slopes. When the slopes are large enough, near 11°, which corresponds to the (105) facets, the islands quickly transform into (105) pyramids, see Fig. 16, with square bases or rectangular bases depending on the film's thickness (the latter occur at larger thicknesses). After some possible coarsening, these islands do no longer coarsen and are 'frozen' in a stationary state, see below. Another remarkable correspondence concerns the correlated growth for thick-enough films (nevertheless thin enough to lead to quantum dots and not dislocations). One finds that both experimentally and theoretically in some conditions, faceted islands grow in groups at some locations while the instability initial corrugation is still developing on the rest of the film. Islands will eventually grow all over the surface [17], but this kind of intermediate state can be found even after 18 h of annealing, see Fig. 17. It may be attributed to the energy barrier between (100) and (105), which must be overcome when the local slopes are large enough, which is the case in the vicinity of large fluctuations. The islands correlations thence keep track of the local fluctuations in the initial linear regime. Note that other anisotropies, such as diffusion or elastic anisotropies, are not considered here as they are expected to contribute more weakly than the surface energy anisotropy.

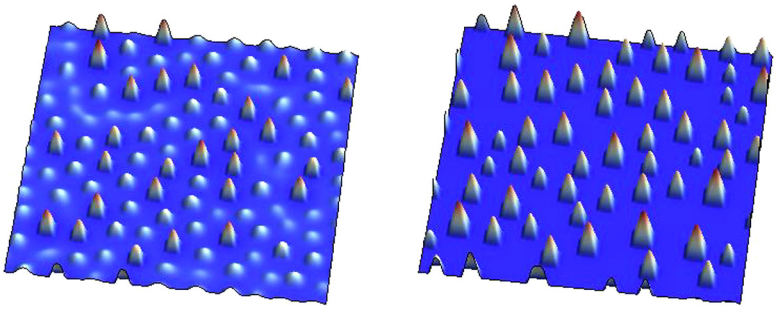

Fig. 16. (Color online.) Evolution of the ATG instability with an anisotropic surface energy $\gamma(\boldsymbol{n})$ dedicated to SiGe, as depicted in Fig. 15.

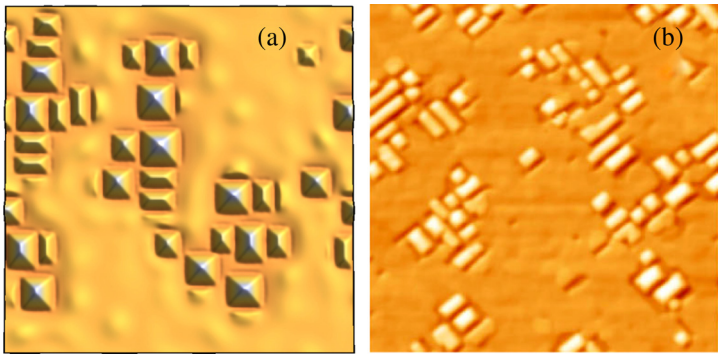

Fig. 17. (Color online.) Intermediate stage of the self-organization dictated by the ATG instability where some quantum dots grow in groups while the linear instability is still growing on the rest of the film (a) in theory and (b) in experiments for a 5-nm $Si_{0.7}Ge_{0.3}$ film on Si(100) annealed for 18 h [17].

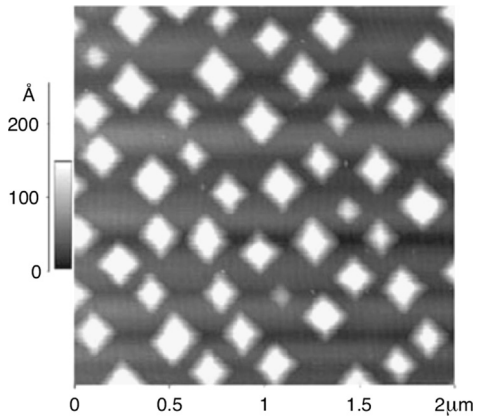

Fig. 18. Atomic force microscopy image of a 5-nm-thick $Si_{0.75}Ge_{0.25}$ film on Si(100), from [72].

5. Directed self-organization

Self-organized quantum dots are investigated for their potential spatial order and uniformity without a potentially detrimental external action. However, the quantum dots resulting from the ATG instability display poor spatial order and significant size dispersion, see, e.g., Fig. 18, which is a serious drawback for their use in large assemblies [2]. Their order and uniformity is poorly enhanced compared to the dots resulting from the intrinsically stochastic nucleation growth. This disappointing result originates from the low order of the ATG linear regime of the instability. Indeed, the ATG growth rate is isotropic and does not lead to a periodic structure, but rather to an initial morphology with already some disorder, see Fig. 5. In addition, after the initial linear regime, the islands undergo some partial coarsening, which favors large islands at the expense of the smaller ones, so that size dispersion again increases.

In order to improve the quantum dot morphological features, growth was processed either on stress pattern, see, e.g., [73], or on morphological patterns [17]. In the latter case, the resulting islands self-organize dramatically in quite perfect arrays, forming meta-crystals of quantum dots [74]. But, at least in the nucleation regime where it was most studied, contradictory experimental results were found in similar conditions on pit-like patterns or on mesas. Islands were found

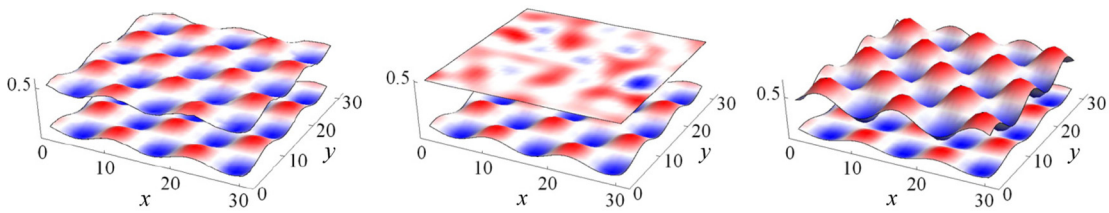

Fig. 19. (Color online.) Evolution of the ATG instability on a pattern with a wavelength equal to the maximum of the ATG growth rate. The film surface, which initially wets the substrate, skips from an in-phase geometry to an out-of-phase geometry, which relaxes the elastic energy more efficiently. From [85].

on the top or at the edge of the pattern in [75–78], on the pattern sidewalls in [79] or inside pits in [79–81]. They were also found inside pits at low temperatures and between pits at high temperatures in [82]. The evolution on top of a morphological pattern results from different and contradictory driving forces. On the one side, the elastic energy minimization for a given island favors its location onto a pit [83,84]. On the other side, growth is dictated by gradients in the surface chemical potential, which includes capillary and elastic contributions. If the elastic contribution from the patterned film/substrate interface is indeed minimum on the top of a pit, the elastic contribution from the free surface is minimum on the top of a corrugation and maximal in its valleys. On the contrary, the surface energy contribution is maximal on the top of a corrugation and minimal in its valleys. Finally, the wetting effects tend to force the film to follow the pattern's shape. Hence, the quantum dot growth on a pattern results form the dynamical competition between these opposite driving forces, whose balance is a priori non-settled.

To investigate these systems, the ATG dynamical equation was generalized in the presence of a patterned film/substrate interface. Similar to the elastic relaxation induced by the surface corrugation that is the ATG driving force, the film/substrate interface introduces elastic dipoles and creates an elastic field that propagates up to the surface. If the interface is located at $z = \eta(\boldsymbol{r})$, one finds an extra contribution in the surface elastic chemical potential, which reads at linear order in the slopes of η [85,86]

$$\mu^{\mathrm{el}}/\mathcal{E}_0 = 1 - 2(1+\nu)\left[\mathcal{H}_{ii}(h) - \mathcal{B}[\mathcal{H}_{ii}(\eta)\right], \tag{11}$$

with summation over repeated indices $i = x, y$. The damping operator is merely given in the Fourier space by $\mathcal{B}(h) = \exp(-|\boldsymbol{k}|\bar{h})h(\boldsymbol{k})$, where $\bar{h}$ is the mean film thickness. This exponential damping in the growth direction occurs over a length scale equal to the horizontal wavelength, as a result of the absence of a length scale in elasticity. The extra term $\mathcal{B}[\mathcal{H}]$ acts as a forcing term on the dynamical equation of the surface. Moreover, the influence of the patterned interface is also at work in two other effects. First, the wetting interactions that are dependent on the film thickness may be locally given through $\gamma = \gamma[h(\boldsymbol{r}) - \eta(\boldsymbol{r})]$, which forces the wetting film to follow the morphology of the pattern. Second, the deposition initially occurs on the patterned substrate so that the film initially follows the pattern's morphology. Hence, the pattern shape η also corresponds to the film initial condition $h(\boldsymbol{r}, t = 0)$, which may be more or less amplified depending on the growth rate σ, which is a function of the pattern's typical length scale and spectrum $\eta(\boldsymbol{k})$. As a result, the linear evolution is characterized by the ratio between the pattern wavelength λ_η and the natural instability wavelength $\lambda_{\mathrm{ATG}} = 8\pi\, l_0/3$, which corresponds to the maximum of $\sigma(|\boldsymbol{k}|)$. Two typical cases arise [85,86]. When $\lambda_\eta \simeq \lambda_{\mathrm{ATG}}$, the evolution is mainly dictated by the λ_{ATG} mode. The initial condition where the film wets the substrate corresponds to a maximum of elastic energy where the film surface is in phase with the substrate. The minimum of energy corresponds to a configuration where the film is out of phase with its substrate [83]. Hence, when the film's thickness is large enough so that wetting effects are negligible, the film skips at a given time t^{ex} from an in-phase geometry to an out-of-phase geometry. This shift occurs for a geometry with a single $\boldsymbol{k}$ through the vanishing of the corrugation amplitude, even though the growth rate σ is maximum for this wavelength, see Fig. 19. On the other hand, when the substrate wavelength is not in the vicinity of λ_{ATG}, the maximum mode grows faster and leads after some time $t^{\max}$ to a surface morphology that is quite similar to the morphology in the absence of the forcing term.

After the initial linear regime, the growth of the quantum dots on a pattern is given by its non-linear evolution. It may be described by an evolution equation similar to the one on a flat substrate (9), but with (i) a forcing term, which can be computed at orders η and η^2, (ii) with a coupling proportional to $h\,\eta$, and (iii) a wetting effect depending on $h(\boldsymbol{r}) - \eta(\boldsymbol{r})$ [87]. One may first study a sinusoidal pattern so that the pattern's effect is governed only by its wavelength λ_η and by the film's thickness $\bar{h}$ that rules the exponential damping of the interface dipoles. When one also adds an ad-hoc anisotropy to describe SiGe systems, one finds again that the islands grow, develop (105) facets, before their coarsening interrupts. The geometric uniformity of the resulting islands can be spectacular. Even with a shallow pattern (i.e. for a pattern slope as small as a few percent), one finds in some conditions a self-organization in meta-crystals of quantum dots, see Fig. 20a–b. However, in some other conditions, the self-organization leads to a poor order similar to the one on a flat substrate, see Fig. 20c. The summary of the localization of the dots when they no longer coarsen is given in the kinetic phase diagram in Fig. 21. The islands' localization can be rationalized kinetically as it coincides with the geometry of the surface when the islands arise from the initial linear instability, i.e. when the linear instability nearly touches the

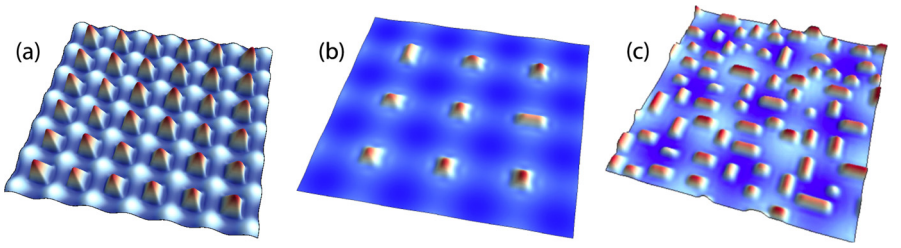

Fig. 20. (Color online.) Quantum dots resulting from the growth of the ATG instability (with a natural wavelength λ_{ATG}) on top of a sinusoidal pattern (with a wavelength λ_η) for (a) $\lambda_\eta \simeq \lambda_{\mathrm{ATG}}$, (b) a large $\lambda_\eta/\lambda_{\mathrm{ATG}}$ and thin film and (c) for a thick film but $\lambda_\eta/\lambda_{\mathrm{ATG}} \gtrsim 2$, from [87].

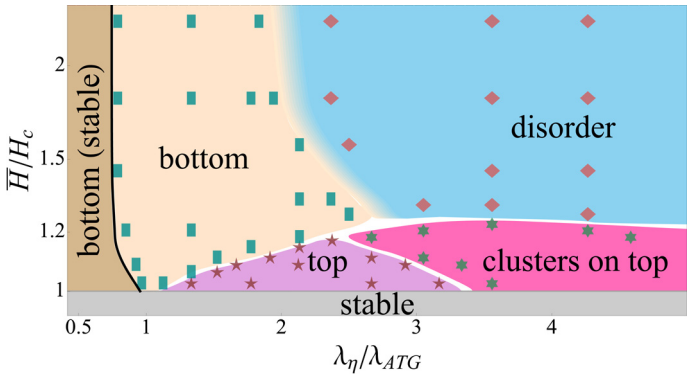

Fig. 21. (Color online.) Kinetic phase diagram giving the localization of the quantum dots with respect to a sinusoidal pattern as a function of the ratio $\lambda_\eta/\lambda_{\mathrm{ATG}}$ of the pattern to instability wavelength and of the film's thickness, from [87].

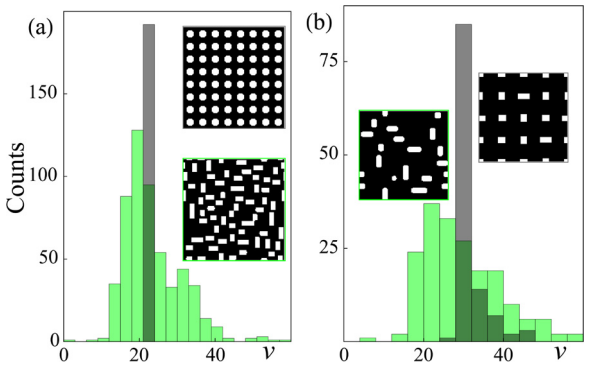

Fig. 22. (Color online.) Island size distribution resulting from the growth on a pattern for the growth (gray) (a) in the valleys and (b) on the hills of the pattern, and (green) on a flat pattern with otherwise similar parameters, from [87].

substrate so that the non-linear growth proceeds. When $\lambda_\eta/\lambda_{\mathrm{ATG}} \simeq 1$, the fastest growing mode is driving the evolution fast; as described above, the linear instability shifts from an in-phase one to an out-of-phase one so that the quantum dots arise when the instability is already out of phase and the dots naturally grow in the valleys of the pattern. For larger $\lambda_\eta/\lambda_{\mathrm{ATG}}$ but smaller than ~ 2, the localization depends on film thickness: when $\bar{h}$ is small, the linear instability promptly approaches the substrate while it is still in-phase, and the dots grow on the top of the pattern; for a larger thickness, the linear instability has time to shift before it approaches the substrate, and the dots grow in the valleys. Finally, for large $\lambda_\eta/\lambda_{\mathrm{ATG}}$, the influence of the pattern is rather small and a mainly disordered geometry is found, similar to the one on a flat substrate, except for quite thin films where the dots still grow on the top of the pattern and gather in clusters of 2 or 3 islands on each top. Note that in some conditions, one may find islands that grow both on the hills and in the valleys of the pattern, the former disappearing to the benefit of the latter, which have a lower elastic energy. The island size distribution in the meta-crystal structures is plotted in Fig. 22, and shows a peaked distribution, significantly improved compared to the case of a flat substrate. Finally, one also finds that the kinetic competition exemplified above for a sinusoidal pattern may rationalize the growth on pit-like patterns by considering the kinetic phase diagram (Fig. 21) with the appropriate length scales [88].

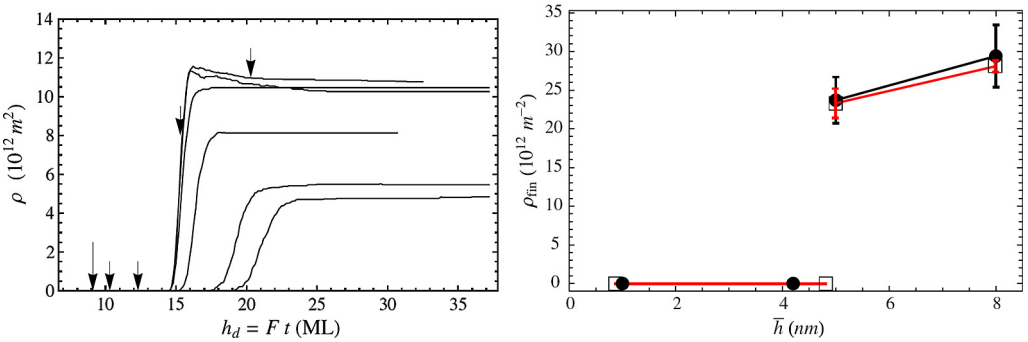

Fig. 23. (Left) Island density as a function of time for (from bottom to top) an increasing film thickness (the arrows show when deposition is stopped and when annealing begins), from [70]. (Right) Island density in the stationary state as a function of film thickness (black) in experiments on a $Si_{0.7}Ge_{0.3}$ film and (red) in the ATG theory with wetting and anisotropy, from [29]. (For interpretation of the references to color in this figure legend, the reader is referred to the web version of this article.)

6. Coarsening

Coarsening is a key issue in quantum dot growth. Usually, large islands have a lower chemical potential, which is already understandable with only capillary effects, as large objects have a lower surface-to-volume ratio. As a consequence, large islands drag matter from the smaller ones and the number of islands decreases with time while their average size increases. This stochastic process is a source of non-uniformity that may be detrimental for the use of assemblies of quantum dots. Its understanding involves the account of dynamical and long-range effects in epitaxial films. However, as explained in the following, the coarsening of the quantum dots enforced by the ATG instability is non-standard and does not follow the classic laws of Ostwald coarsening [89,90].

Ostwald ripening is generally characterized by power laws that depend on the physics at work. In the seminal article by Lifshitz and Slyozov where diffusion is the limiting process [91], the particle mean size increases as t^{α}, with $\alpha = 1/3$, while the particle density decreases as $1/t^{\zeta}$, with $\zeta = 1$. In fact, their analysis concerns 3D objects evolving due to capillary effects and with a diffusion that occurs in 3D, but it was extended to 2D objects and/or 2D diffusion [91–94]. For the coarsening of 3D objects via 2D diffusion, one finds $\zeta = \frac{3}{4}$ and $\alpha = \frac{1}{4}$.[1]

As regards ATG instability, its evolution on isotropic systems does indeed lead to a non-interrupted coarsening where large islands grow, see, e.g., Fig. 9. But the resulting ripening deviates from the usual laws of Ostwald's coarsening and is significantly faster. The standard non-linear analysis described by (9) with regular wetting interactions leads to $\zeta = 1.3$ and a surface roughness w that increases as t^{β} with $\beta = 0.7$ [53].[2] The increase in the coarsening speed compared to the laws of Ostwald ripening is not surprising due to the presence of elasticity, which introduces long-range effects and a subtle dependence of the islands' energy on their volume. Especially, as the islands grow, their aspect ratio (height to base ratio) increases so that the larger islands relax the elastic strain more efficiently [53]. As a consequence, in addition to capillary effects, elasticity adds in strained films another driving force when the island shape is free to evolve.

An entirely different picture is found however as soon as anisotropy comes into play. Indeed, the islands shapes are then dictated by surface effects and given by the materials properties: (105) pyramids, then domes and super-domes with (113) and (15 3 23) facets. The evolution between these shapes was first argued to be a first-order transition [96] before experimental real-time analysis exhibited a rather anomalous coarsening [97]. But we focus here on the first anisotropic shapes that are (105) pyramids that solely occur when the film's thickness is not too large. As described in Section 4, when one considers a surface energy that favors (105) facets in the ATG evolution, one finds the self-organization of (105) pyramids. But contrary to the isotropic ones, after some partial coarsening, these pyramids no longer coarsen, see, e.g., Fig. 23. This interruption for moderate film thicknesses (not too large so that domes do not form) was also found in experiments, even for annealing times as large as three days [47,29]. As a result, the pyramid density in this stationary state is given merely by film thickness, see Fig. 23. The coarsening interruption or significant slowdown may be related to different effects. On the one side, when the pyramids are well defined, elasticity is no longer a driving force for coarsening. Indeed, when the pyramid shape is given, its volume can increase only by a self-similar evolution so that the elastic energy is exactly proportional to the volume. Consequently, the elastic chemical potential does not depend on the volume and does not contribute to surface chemical potential gradients. On the other side, capillary effects, which should a priori favor large islands, also involve here wetting interactions. If one computes the energetic pathway that describes coarsening between two islands, accounting for an elastic energy proportional to the volume and a surface energy with wetting effects, one finds the energetic profile typically depicted in Fig. 24. The energy landscape is noticeably characterized by a valley of states as the total energy increases due to wetting interactions when large volumes start to consume the wetting layer. In this valley,

[1] Note that when coarsening is limited by attachment/detachment one finds $\langle R \rangle \sim t^{1/2}$ [95].

[2] A weakly non-linear analysis coupled with singular $1/h^2$ wetting interactions lead to $\beta = 2.8$ [27].

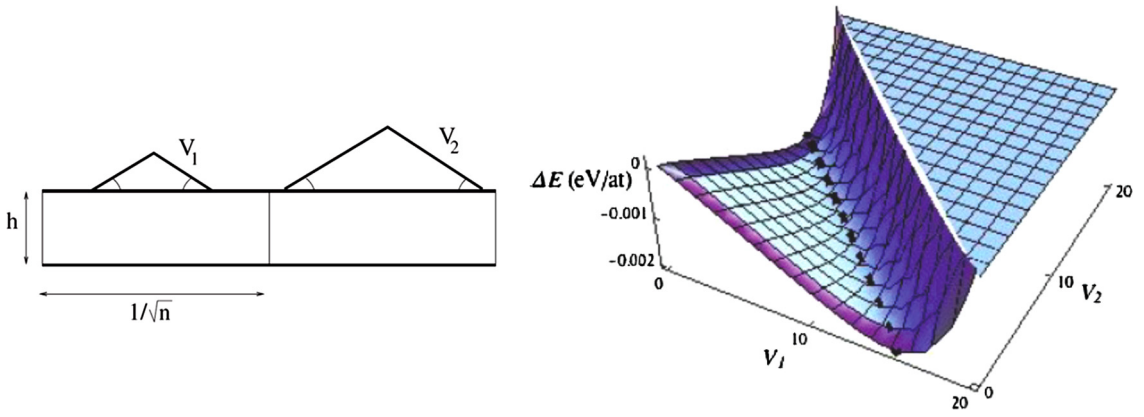

Fig. 24. (Left) Two islands of volumes V_1 and V_2 sitting on a wetting layer of thickness h; (right) energy landscape as a function of V_1 and V_2 accounting for elastic, surface and wetting energies, from [70].

the true minimum is well for a vanishing V_1 or V_2 (complete coarsening); but the energy differences are so small in this valley that the islands are likely to be glued in this valley [70]. Note that when the film thickness is large enough, some large islands transform into domes and coarsening acts again, as domes have lower chemical potential.

7. Conclusion

We describe in this article the self-organization of quantum dots resulting from the Asaro–Tiller–Grinfel'd instability. The latter is driven by the misfit strain relaxation allowed by surface morphological evolution. We describe how its development into quantum dots in epitaxial strained films is captured in some conditions by the basic mechanisms of the instability, but involves ingredients specific to these systems, such as wetting interactions or crystalline anisotropy. Their account allows us to rationalize experimental outcomes: quantum dots vs. dislocation, critical thickness for evolution, formation of faceted objects, dependance on substrate orientation, effects of patterns, coarsening dynamics etc. If the basic aspects of the quantum dot growth are now rather well understood, many questions are still left open:

- (i) coupling between alloying effects and the dynamical evolution: how the latter drives composition inhomogeneities in the dots but also how composition differences may drive the morphological evolution. This issue is crucial for the use of quantum dots in devices as inhomogeneities may significantly modify the dots' properties;
- (ii) crossover between the nucleation and the instability regimes, which are clearly different initial stages that however lead to subsequent similar evolutions;
- (iii) the influence of geometry on long-range elastic interactions, especially on geometries under scrutiny in experiments, nano-membranes, nano-wires, etc. The latter are investigated not only for the use of new geometries, but also for the potential control over the nanostructures electronic properties. The improved control over the promising quantum dots properties clearly appeal for a better understanding and control of their growth.

References

[1] F.A. Zwanenburg, A.S. Dzurak, A. Morello, M.Y. Simmons, L.C.L. Hollenberg, G. Klimeck, S. Rogge, S.N. Coppersmith, M.A. Eriksson, Silicon quantum electronics, Rev. Mod. Phys. 85 (2013) 961, http://link.aps.org/doi/10.1103/RevModPhys.85.961.
[2] J.-M. Baribeau, X. Wu, N.L. Rowell, D.J. Lockwood, Ge dots and nanostructures grown epitaxially on Si, J. Phys. Condens. Matter 18 (2006) R139.
[3] D.D. Vvedensky, Quantum dots: self-organized and self-limiting structures, in: A.V. Narlikar, Y.Y. Fu (Eds.), Oxford Handbook of Nanoscience and Technology, vol. 3, Oxford University Press, Oxford, England, 2010, p. 205.
[4] Z.I. Alferov, R.F. Kazarinov, I. Alferov, et al., Authors certificate 28448, U.S.S.R.Zh., Sov. Phys., Solid State 9 (1967) 208.
[5] H. Kroemer, A proposed class of heterojunction injection lasers, Proc. IEEE 51 (1963) 1782.
[6] Efficient blue light-emitting diodes leading to bright and energy-saving white light sources, The Royal Swedish Academy of Sciences, 7 Oct. 2014.
[7] R.J. Asaro, W.A. Tiller, Interface morphology development during stress-corrosion cracking: Part 1: via surface diffusion, Metall. Trans. 3 (1972) 1789.
[8] M.A. Grinfel'd, Instability of the separation boundary between a nonhydrostatiscally stressed elastic body and a melt, Sov. Phys. Dokl. 31 (1986) 831.
[9] M. Thiel, A. Willibald, P. Evers, A. Levchenko, P. Leiderer, S. Balibar, Stress-induced melting and surface instability of ^{4}He crystals, Europhys. Lett. 20 (1992) 707.
[10] S. Balibar, H. Alles, A.Y. Parshin, Helium crystals under stress: the Grinfeld instability, Rev. Mod. Phys. 77 (2005) 317.
[11] J. Bodensohn, K. Nicolai, P. Leiderer, The growth of atomically rough ^{4}He crystals, Z. Phys. B, Condens. Matter 64 (1986) 55.
[12] J. Berréhar, C. Caroli, C. Lapersonne-Meyer, M. Schott, Surface patterns on single-crystal films under uniaxial stress: experimental evidence for the Grinfeld instability, Phys. Rev. B 46 (1992) 13487.
[13] J.Y. Yao, T.G. Andersson, G.L. Dunlop, Structure of lattice-strained $In_xGa_{1-x}As/GaAs$ layers studied by transmission electron microscopy, Appl. Phys. Lett. 53 (1988) 1420.
[14] A.J. Pidduck, D.J. Robbins, A.G. Cullis, W.Y. Leong, A.M. Pitt, Evolution of surface morphology and strain during SiGe epitaxy, Thin Solid Films 222 (1992) 78.

[15] H. Gao, W. Nix, Surface roughening of heteroepitaxial thin film, Annu. Rev. Mater. Sci. 29 (1999) 173.
[16] P. Politi, G. Grenet, A. Marty, A. Ponchet, J. Villain, Instabilities in crystal growth by atomic or molecular beams, Phys. Rep. 324 (2000) 271.
[17] J.-N. Aqua, I. Berbezier, L. Favre, T. Frisch, A. Ronda, Growth and self-organization of SiGe nanostructures, Phys. Rep. 522 (2013) 59, http://dx.doi.org/10.1016/j.physrep.2012.09.006, http://www.sciencedirect.com/science/article/pii/S0370157312002761.
[18] C. Teichert, Self organization of nanostructures in semiconductor heteroepitaxy, Phys. Rep. 365 (2002) 335.
[19] B.J. Spencer, P.W. Voorhees, S.H. Davies, Morphological instability in epitaxially strained dislocation-free solid films: linear stability theory, J. Appl. Phys. 73 (1993) 4955.
[20] P.H. Leo, R.F. Sekerka, The effect of surface stress on crystal–melt and crystal–crystal equilibrium, Acta Metall. 37 (1989) 3119.
[21] W.W. Mullins, Theory of thermal grooving, J. Appl. Phys. 28 (1957) 333.
[22] J. Tersoff, B.J. Spencer, A. Rastelli, H. von Känel, Barrierless formation and faceting of SiGe islands on Si(001), Phys. Rev. Lett. 89 (2002) 196104, http://link.aps.org/doi/10.1103/PhysRevLett.89.196104.
[23] G. Wulff, Zur Frage der Geschwindigkeit des Wachsthums und der Auflösung der Krystallfläschen, Z. Kristallogr. 34 (1901) 449.
[24] C.-H. Chiu, H. Gao, A numerical study of stress controlled surface diffusion during epitaxial film growth, in: S.P. Baker, et al. (Eds.), Thin Films: Stresses and Mechanical Properties V, in: MRS Symposia Proceedings, vol. 356, Materials Research Society, Pittsburgh, 1995, p. 33.
[25] P. Müller, R. Kern, The physical origin of the two-dimensional towards three-dimensional coherent epitaxial Stranski–Krastanov transition, Appl. Surf. Sci. 102 (1996) 6, http://www.sciencedirect.com/science/article/pii/0169433296000098.
[26] B.J. Spencer, P.W. Voorhees, S.H. Davis, Morphological instability in epitaxially strained dislocation-free solid films, Phys. Rev. Lett. 67 (1991) 3696, http://link.aps.org/doi/10.1103/PhysRevLett.67.3696.
[27] M.S. Levine, A.A. Golovin, S.H. Davis, P.W. Voorhees, Self-assembly of quantum dots in a thin epitaxial film wetting an elastic substrate, Phys. Rev. B 75 (2007) 205312, http://link.aps.org/doi/10.1103/PhysRevB.75.205312.
[28] C.-H. Chiu, H. Gao, Stress singularities along a cycloid rough surface, Int. J. Solids Struct. 30 (1993) 2983.
[29] J.-N. Aqua, A. Gouyé, A. Ronda, T. Frisch, I. Berbezier, Interrupted self-organization of SiGe pyramids, Phys. Rev. Lett. 110 (2013) 096101, http://link.aps.org/doi/10.1103/PhysRevLett.110.096101.
[30] I. Berbezier, J.-N. Aqua, M. Aouassa, L. Favre, S. Escoubas, A. Gouyé, A. Ronda, Accommodation of SiGe strain on a universally compliant porous silicon substrate, Phys. Rev. B 90 (2014) 035315, http://link.aps.org/doi/10.1103/PhysRevB.90.035315.
[31] J.-N. Aqua, L. Favre, A. Ronda, A. Benkouider, I. Berbezier, Configurable compliant substrates for SiGe nanomembrane fabrication, Cryst. Growth Des. 15 (2015) 3399, http://dx.doi.org/10.1021/acs.cgd.5b00485.
[32] P. Sutter, M.G. Lagally, Nucleationless three-dimensional island formation in low-misfit heteroepitaxy, Phys. Rev. Lett. 84 (2000) 4637, http://link.aps.org/doi/10.1103/PhysRevLett.84.4637.
[33] C. Ratsch, P. Smilauer, D.D. Vvedensky, A. Zangwill, Mechanism for coherent island formation during heteroepitaxy, J. Phys. I (France) 6 (1996) 575.
[34] Y. Chen, J. Washburn, Structural transition in large-lattice-mismatch heteroepitaxy, Phys. Rev. Lett. 77 (1996) 4046.
[35] C.-H. Lam, C.-K. Lee, L.M. Sander, Competing roughening mechanisms in strained heteroepitaxy: a fast kinetic Monte Carlo study, Phys. Rev. Lett. 89 (2002) 216102, http://link.aps.org/doi/10.1103/PhysRevLett.89.216102.
[36] J. Villain, Kinetic aspects of thermodynamical instabilities, C. R. Phys. 4 (2003) 201, http://dx.doi.org/10.1016/S1631-0705(03)00002-1, http://www.sciencedirect.com/science/article/pii/S1631070503000021.
[37] J.-N. Aqua, A. Gouyé, T. Auphan, T. Frisch, A. Ronda, I. Berbezier, Orientation dependence of the elastic instability on strained SiGe films, Appl. Phys. Lett. 98 (2011) 161909, http://dx.doi.org/10.1063/1.3576916.
[38] A. Vailionis, B. Cho, G. Glass, P. Desjardins, D.G. Cahill, J.E. Greene, Pathway for the strain-driven two-dimensional to three-dimensional transition during growth of Ge on Si(001), Phys. Rev. Lett. 85 (2000) 3672.
[39] B.J. Spencer, D.I. Meiron, Nonlinear evolution of the stress-driven morphological instability in a two-dimensional semi-infinite solid, Acta Metall. Mater. 42 (1994) 3629.
[40] W.H. Yang, D.J. Srolovitz, Cracklike surface instabilities in stressed solids, Phys. Rev. Lett. 71 (1993) 1593, http://link.aps.org/doi/10.1103/PhysRevLett.71.1593.
[41] A.A. Golovin, S.H. Davis, P.W. Voorhees, Self-organization of quantum dots in epitaxially strained solid films, Phys. Rev. E 68 (2003) 056203, http://link.aps.org/doi/10.1103/PhysRevE.68.056203.
[42] P. Nozières, Shape and growth of crystals, in: C. Godrèche (Ed.), Solids far from Equilibrium, Cambridge University Press, Cambridge, 1991, p. 1.
[43] J. Tersoff, Stress-induced layer-by-layer growth of Ge on Si(100), Phys. Rev. B 43 (1991) 9377, http://link.aps.org/doi/10.1103/PhysRevB.43.9377.
[44] G.-H. Lu, F. Liu, Towards quantitative understanding of formation and stability of Ge hut islands on Si(001), Phys. Rev. Lett. 94 (2005) 176103, http://link.aps.org/doi/10.1103/PhysRevLett.94.176103.
[45] M.J. Beck, A. van de Walle, M. Asta, Surface energetics and structure of the Ge wetting layer on Si(100), Phys. Rev. B 70 (2004) 205337, http://link.aps.org/doi/10.1103/PhysRevB.70.205337.
[46] J.W. Matthews, A.E. Blakeslee, Defects in epitaxial multilayers, I: misfit dislocations, J. Cryst. Growth 27 (1974) 118.
[47] I. Berbezier, A. Ronda, A. Portavoce, SiGe nanostructures: new insights into growth processes, J. Phys. Condens. Matter 14 (2002) 8283.
[48] J.A. Floro, E. Chason, R.D. Twesten, R.Q. Hwang, L.B. Freund, SiGe coherent islanding and stress relaxation in the high mobility regime, Phys. Rev. Lett. 79 (1997) 3946.
[49] C.S. Ozkan, W.D. Nix, H. Gao, Strain relaxation and defect formation in heteroepitaxial $Si_{1-x}Ge_x$ films via surface roughening induced by controlled annealing experiments, Appl. Phys. Lett. 70 (1997) 2247.
[50] I. Berbezier, B. Gallas, A. Ronda, J. Derrien, Dependence of SiGe growth instability on Si substrate orientation, Surf. Sci. 412 (1998) 415.
[51] R.M. Tromp, F.M. Ross, M.C. Reuter, Instability-driven SiGe island growth, Phys. Rev. Lett. 84 (2000) 4641, http://link.aps.org/doi/10.1103/PhysRevLett.84.4641.
[52] Y. Pang, R. Huang, Nonlinear effect of stress and wetting on surface evolution of epitaxial thin films, Phys. Rev. B 74 (2006) 075413.
[53] J.-N. Aqua, T. Frisch, A. Verga, Nonlinear evolution of a morphological instability in a strained epitaxial film, Phys. Rev. B 76 (2007) 165319, http://link.aps.org/doi/10.1103/PhysRevB.76.165319.
[54] C.G. Gamage, Z.-F. Huang, Nonlinear dynamics of island coarsening and stabilization during strained film heteroepitaxy, Phys. Rev. B 87 (2013) 022408.
[55] L.-H. Tang, Island formation in submonolayer epitaxy, J. Phys. I (France) 3 (1993) 935.
[56] A. Pimpinelli, J. Villain, Physics of Crystal Growth, Cambridge University Press, 1998.
[57] D.J. Eaglesham, A.E. White, L.C. Feldman, N. Moriya, D.C. Jacobson, Equilibrium shape of Si, Phys. Rev. Lett. 70 (1993) 1643.
[58] J.M. Bermond, J.J. Métois, X. Egéa, F. Floret, The equilibrium shape of silicon, Surf. Sci. 330 (1995) 48.
[59] C.J. Moore, C.M. Retford, M.J. Beck, M. Asta, M.J. Miksis, P.W. Voorhees, Orientation dependence of strained-Ge surface energies near (001): role of dimer–vacancy lines and their interactions with steps, Phys. Rev. Lett. 96 (2006) 126101.
[60] A. Rastelli, H. Von Känel, B.J. Spencer, J. Tersoff, Prepyramid-to-pyramid transition of SiGe islands on Si(001), Phys. Rev. B 68 (2003) 115301.
[61] Y.W. Mo, D.E. Savage, B.S. Swartzentruber, M.G. Lagally, Kinetic pathway in Stranski–Krastanov growth of Ge on Si(001), Phys. Rev. Lett. 65 (1990) 1020, http://link.aps.org/doi/10.1103/PhysRevLett.65.1020.
[62] P. Gaillard, J.-N. Aqua, T. Frisch, Kinetic Monte Carlo simulations of the growth of silicon germanium pyramids, Phys. Rev. B 87 (2013) 125310, http://link.aps.org/doi/10.1103/PhysRevB.87.125310.

[63] A. Rastelli, M. Kummer, H. von Känel, Reversible shape evolution of Ge islands on Si(001), Phys. Rev. Lett. 87 (2001) 256101.
[64] A.A. Golovin, S.H. Davis, A.A. Nepomnyashchy, Model for faceting in a kinetically controlled crystal growth, Phys. Rev. E 59 (1999) 803.
[65] H.R. Eisenberg, D. Kandel, Wetting layer thickness and early evolution of epitaxially strained thin films, Phys. Rev. Lett. 85 (1999) 1286.
[66] Y.W. Zhang, Self-organization, shape transition, and stability of epitaxially strained islands, Phys. Rev. B 61 (2000) 10388.
[67] Y. Xiang, W. E, Nonlinear evolution equation for the stress-driven morphological instability, J. Appl. Phys. 91 (2002) 9414.
[68] A. Ramasubramaniam, V.B. Shenoy, Three-dimensional simulations of self-assembly of hut-shaped Si–Ge quantum dots, J. Appl. Phys. 95 (2004) 7813.
[69] C.-H. Chiu, Z. Huang, Numerical simulation for the formation of nanostructures on the Stranski–Krastanow systems by surface undulation, J. Appl. Phys. 101 (2007) 113540.
[70] J.-N. Aqua, T. Frisch, Influence of surface energy anisotropy on the dynamics of quantum dot growth, Phys. Rev. B 82 (2010) 085322, http://link.aps.org/doi/10.1103/PhysRevB.82.085322.
[71] http://www.insp.jussieu.fr/Films.html [online link].
[72] I. Berbezier, A. Ronda, F. Volpi, A. Portavoce, Morphological evolution of SiGe layers, Surf. Sci. 531 (2003) 231.
[73] F. Leroy, J. Eymery, P. Gentile, F. Fournel, Ordering of Ge quantum dots with buried Si dislocation networks, Appl. Phys. Lett. 80 (2002) 3078, http://scitation.aip.org/content/aip/journal/apl/80/17/10.1063/1.1474601.
[74] M. Grydlik, G. Langer, T. Fromherz, F. Schäffler, M. Brehm, Recipes for the fabrication of strictly ordered Ge islands on pit-patterned Si(001) substrates, Nanotechnology 24 (2013) 105601, http://stacks.iop.org/0957-4484/24/i=10/a=105601.
[75] G. Jin, J.L. Liu, S.G. Thomas, Y.H. Luo, K.L. Wang, B.-Y. Nguyen, Controlled arrangement of self-organized Ge islands on patterned Si (001) substrates, Appl. Phys. Lett. 75 (1999) 2752, http://link.aip.org/link/?APL/75/2752/1.
[76] T. Kitajima, B. Liu, S.R. Leone, Two-dimensional periodic alignment of self-assembled Ge islands on patterned Si(001) surfaces, Appl. Phys. Lett. 80 (2002) 497, http://link.aip.org/link/?APL/80/497/1.
[77] B. Yang, F. Liu, M.G. Lagally, Local strain-mediated chemical potential control of quantum dot self-organization in heteroepitaxy, Phys. Rev. Lett. 92 (2004) 025502, http://link.aps.org/doi/10.1103/PhysRevLett.92.025502.
[78] P.D. Szkutnik, A. Sgarlata, S. Nufris, N. Motta, A. Balzarotti, Real-time scanning tunneling microscopy observation of the evolution of Ge quantum dots on nanopatterned Si(001) surfaces, Phys. Rev. B 69 (2004) 201309, http://link.aps.org/doi/10.1103/PhysRevB.69.201309.
[79] Z. Zhong, A. Halilovic, M. Muhlberger, F. Schaffler, G. Bauer, Ge island formation on stripe-patterned Si(001) substrates, Appl. Phys. Lett. 82 (2003) 445, http://link.aip.org/link/?APL/82/445/1.
[80] M. Bollani, D. Chrastina, A. Fedorov, R. Sordan, A. Picco, E. Bonera, Ge-rich islands grown on patterned Si substrates by low-energy plasma-enhanced chemical vapour deposition, Nanotechnology 21 (2010) 475302, http://stacks.iop.org/0957-4484/21/i=47/a=475302.
[81] Y.J. Ma, Z. Zhong, X.J. Yang, Y.L. Fan, Z.M. Jiang, Factors influencing epitaxial growth of three-dimensional Ge quantum dot crystals on pit-patterned Si substrate, Nanotechnology 24 (2013) 015304, http://stacks.iop.org/0957-4484/24/i=1/a=015304.
[82] I. Berbezier, A. Ronda, SiGe nanostructures, Surf. Sci. Rep. 64 (2009) 47, http://www.sciencedirect.com/science/article/pii/S0167572908000769.
[83] H. Wang, Y. Zhang, F. Liu, Enhanced growth instability of strained film on wavy substrate, J. Appl. Phys. 104 (2008) 054301, http://dx.doi.org/10.1063/1.2968223.
[84] G. Katsaros, J. Tersoff, M. Stoffel, A. Rastelli, P. Acosta-Diaz, G.S. Kar, G. Costantini, O.G. Schmidt, K. Kern, Positioning of strained islands by interaction with surface nanogrooves, Phys. Rev. Lett. 101 (2008) 096103, http://link.aps.org/doi/10.1103/PhysRevLett.101.096103.
[85] X. Xu, J.-N. Aqua, T. Frisch, Growth kinetics in a strained crystal film on a wavy patterned substrate, J. Phys. Condens. Matter 24 (2012) 045002, http://stacks.iop.org/0953-8984/24/i=4/a=045002.
[86] X. Xu, J.-N. Aqua, T. Frisch, Growth of a strained epitaxial film on a patterned substrate, C. R. Phys. 14 (2013) 199, http://dx.doi.org/10.1016/j.crhy.2012.11.006.
[87] J.N. Aqua, X. Xu, Directed self-organization of quantum dots, Phys. Rev. E 90 (2014) 030402, http://link.aps.org/doi/10.1103/PhysRevE.90.030402.
[88] J.-N. Aqua, X. Xu, Growth of quantum dots on pit-patterns, Surf. Sci. 639 (2015) 20, http://dx.doi.org/10.1016/j.susc.2015.04.010, http://www.sciencedirect.com/science/article/pii/S0039602815001016.
[89] J.A. Floro, M.B. Sinclair, E. Chason, L.B. Freund, R.D. Twesten, R.D. Hwang, G.A. Lucadamo, Novel SiGe island coarsening kinetics: Ostwald ripening and elastic interactions, Phys. Rev. Lett. 84 (2000) 701, http://link.aps.org/doi/10.1103/PhysRevLett.84.701.
[90] P. Politi, Coarsening dynamics at unstable crystal surfaces, C. R. Phys. 16 (2015) 280.
[91] I.M. Lifshitz, V.V. Slyozov, The kinetics of precipitation from supersaturated solid solutions, J. Phys. Chem. Solids 19 (1961) 35.
[92] J.A. Marqusee, J. Chem. Phys. 81 (1984) 976.
[93] M. Zinke-Allmang, Thin Solid Films 346 (1999) 1.
[94] G. Prévot, Ostwald ripening of three-dimensional clusters on a surface studied with an ultrafast kinetic Monte Carlo algorithm, Phys. Rev. B 84 (2011) 045434, http://link.aps.org/doi/10.1103/PhysRevB.84.045434.
[95] I.M. Lifshitz, V.V. Slyozov, J. Phys. Chem. Solids 19 (1961) 35.
[96] V.A. Shchukin, N.N. Ledentsov, P.S. Kop'ev, D. Bimberg, Spontaneous ordering of arrays of coherent strained islands, Phys. Rev. Lett. 75 (1995) 2968.
[97] A. Rastelli, M. Stoffel, J. Tersoff, G.S. Kar, O.G. Schmidt, Kinetic evolution and equilibrium morphology of strained islands, Phys. Rev. Lett. 95 (2005) 026103, http://link.aps.org/doi/10.1103/PhysRevLett.95.026103.